Water vapor adsorption on Mars

Savijärvi, Hannu

2021-03-15

Savijärvi , H & Harri , A-M 2021 , ' Water vapor adsorption on Mars ' , Icarus , vol. 357 , 114270 . https://doi.org/10.1016/j.icarus.2020.114270

http://hdl.handle.net/10138/351915
https://doi.org/10.1016/j.icarus.2020.114270

Water vapor adsorption on Mars

H. I. Savijärvi[1,2,*], A.-M. Harri[2]

[1]Institute for Atmospheric and Earth System Research / Physics, University of Helsinki, Finland
[2]Finnish Meteorological Institute, Helsinki, Finland

revision 2

30 October 2020

Abstract

Near-surface air moisture observations from Phoenix and Curiosity display diurnal adsorption, which appears insensitive to mineralogy of regolith. To study this, adsorptive column model simulations are made for midsummer at Phoenix, validated against recalibrated TECP water vapor pressures *p*. Two standard-form (= obeying the van't Hoff equilibrium law) adsorption isotherms with quite different specific surface areas A_s do produce nearly identical and good matches with the observed *p*, whereas a widely used non-standard isotherm fails. When made standard, it also produces good results. Adsorbed amounts differ in the three good simulations but their surface fluxes and surface vapor concentrations are nevertheless nearly identical. Properties of regolith except enthalpy are shown to disappear in the model's adsorption term, explaining insensitivity to A_s. The van't Hoff plot of observed *ln p* vs. model's $1/T_g$ during adsorption and desorption suggests enthalpy of about 22 kJ/mol. Enthalpies of the three standard-form isotherms are close to this, explaining their excellent match with each other and with observations. Hence the low-pressure water vapor adsorption to martian regolith appears essentially nonspecific and is associated with low enthalpy, as is typical for physisorption in general.

Keywords: Mars, climate; Mars, surface; Meteorology

*Corresponding author: INAR/Physics, Faculty of Science, 00014 University of Helsinki, Finland

E-mail address: hannu.savijarvi@helsinki.fi

Tel: +358-40-938085

1. Introduction

Mars' desert-like surface is swept by dusty winds. The martian plains are hence generally covered by a layer of porous dusty regolith. For instance, the footpads of Viking lander 1 were buried into the soft regolith to a depth of a few cm (Paton et al., 2016). However, the rockier areas may be partly free of dust, as shown by the Curiosity rover findings along its track on the Gale crater (e.g. Vasavada et al., 2017). Porous regolith was shown in e.g. Jakosky et al. (1997) to deplete water vapor from the martian air at nighttime. This was based on indirect data from the Viking landers 1 and 2 (these landers did not carry moisture instruments). The nocturnal depletion could be due to adsorption of water vapor onto cool regolith. Jakosky et al. hence used a single-column model (SCM) with an adsorption scheme of Zent et al. (1993), obtaining depletion of the observed magnitude. Böttger et al. (2005) and Steele et al. (2017) adopted the Zent scheme for GCM and mesoscale model purposes. In the present study another soil scheme, which assumes adsorption in instantaneous equilibrium, is coupled to the University of Helsinki/Finnish Meteorological Institute (UH/FMI) atmospheric SCM. The results are compared to the available direct *in-situ* observations of martian moisture.

The first *in-situ* moisture instrument on Mars was the Thermal and Electrical Conductivity Probe TECP (Zent et al., 2010; 2016) onboard the polar Phoenix lander at 68ºN. It carried relative humidity and temperature sensors on the electronics board of the ventilated TECP box, which was fixed to a movable robotic arm. Measurements of board-air RH and T (RH_b, T_b) were hence made at different heights, from about 3 cm (~near-surface) up to 150 cm (air) from the surface. The ambient water vapor partial pressure p at the current height is then estimated from $p = RH_b \cdot p_{sat}(T_b)$. Calibration proved to be a problem. Fischer et al. (2019) recently used a spare copy of TECP in a test chamber for recalibration of raw RH_b data. They described the device, methods, results and error analysis in detail, so this is not repeated here. The TECP vapor pressures clearly indicate depletion of moisture every evening at Phoenix (Zent et al., 2010; Fischer et al., 2019). In Savijärvi et al. (2020b) the Fischer et al. *p*-data were used for a basic validation of the UH/FMI SCM. Here this is continued, now comparing four different adsorption isotherm candidates for the martian regolith around Phoenix.

The Mars Science Laboratory (MSL) included the next *in-situ* moisture instrument in its REMS suite (Gomez-Elvira et al., 2012, Harri et al., 2014) onboard the equatorial Curiosity rover in the Gale crater at 4.6ºS. The REMS-H device measures *RH* and *T* at 1.6 m height. With observations of surface air pressure *P* the water vapor volume mixing ratio (*vmr = p(RH,T)/P*) can then be derived (Harri et al., 2014). The MSL *vmr* observations now cover four martian years along the ~25 km track of Curiosity. They, too, display depletion of air water vapor every evening, minimum values of *vmr* and *p* occurring near dawn, when the surface and air are cold (and the measured values of RH are at their highest and most accurate, Harri et al., 2014; Martinez et al., 2017). Hence the daily pre-dawn minima of REMS-H *vmr* and *T* tend to go hand in hand. Figure 1 displays them for the first three martian years, MSL sols 1-2006. The first two and half annual cycles appear to be quite similar in Fig. 1, but from about sol 1800 onward both min *vmr* and min *T* begin to increase. This was shown in Savijärvi et al. (2019b) to be due to the fact that Curiosity then left the crater base and started to climb the bedrock-dominated slopes of Mt. Sharp, encountering higher thermal inertias (*I)*

and very low porosities, and thus higher nocturnal temperatures and much smaller depletion than over the regolith-dominated crater base.

Another noteworthy aspect in Fig. 1 is that although Curiosity recorded regions of quite variable regolith (indicated e.g. by the REMS-observed ground temperatures T_g; Vasavada et al., 2017), the daily minima of *vmr* do not appear to react. For instance, two high-*I* rocky regions (solid lines) and two low-*I* dune regions (dashed lines) are marked in Fig. 1, yet the values of min *vmr* appear to be much the same during these sols as they are in the surrounding sols. The values of min *vmr* appear mainly to follow the daily min *T* (which naturally adjusts to min T_g) rather than to otherwise react to the quite variable mineralogy of the ground along the track.

Yet another aspect is that the single-column and mesoscale models, which have had an adsorption mechanism, tend to produce very similar diurnal *vmr* cycles for adsorption isotherms, which have been measured from widely different proxies for the martian regolith. In other words, water vapor adsorption to martian regolith appears to be largely material-independent (i.e., nonspecific). We consider this aspect in the following, discussing adsorption physics and Earth and Mars observations and making SCM experiments for the PHX warm season.

2. Adsorption physics, Earth observations and laboratory measurements

Physical adsorption (physisorption) of water vapor on dry Mars and Earth desertlike landscapes is an easily reversible surface process, in which water molecules from the air collect onto surfaces of grains in the porous topsoil, due to weak attractive van der Waal-type forces. This is enhanced by low temperatures, when thermal motions are weak. Hence adsorption tends to deplete moisture from the air during evening and night, when temperatures are low but above the dew or frost point. Sunlight warms the topsoil in the morning and increasing thermal motions then drive the weakly attached water molecules back to the air from the soil in desorption. Chemical and phase changes are not involved and the soil and air temperature changes due to the weak process are insignificant.

Adsorption on Earth's semi-arid deserts was documented by Agam and Berliner (2004). They measured moisture variations in sandy bare topsoil (porosity 0.45) in the Negev desert of Israel during the dry season, when dew and rain did not occur. Soil moisture nevertheless varied diurnally, the 0-1 cm layer typically containing water by 1.1 weight-% each afternoon but 2.2% at sunrise. The top 10-cm column soil water content was 0.01 mm in the afternoon but about 0.25 mm at sunrise. This corresponds to a diurnal variation of about 1% of the current air column precipitable water content (PWC). Similar findings have since been made elsewhere. For instance, Masiello et al. (2014) report systematic day-night variation of ground IR emissivity in satellite data over Sahara. These arise from the diurnal moisture variation in the topsoil, due to the daily adsorption and desorption. Suitable day-night orbit IR data could thus be used to chart the diurnal topsoil moisture variation over deserts. Recently even devices applying high-porosity material have been constructed to wring drinkable water from desert air, by utilizing adsorption/desorption. Perhaps these findings could also be applied on Mars.

In laboratory experiments, adsorption onto various materials (typically mineral powders of soil) is measured in constant temperature T_o, while increasing and decreasing the partial pressure p of water vapor. The measured adsorbed amount a of water (in weight-%, or kg water per m^3 of soil) as the function of p is then given as an 'adsorption isotherm'. The oldest empirical Freundlich isotherm, $a(p,T_o) \sim A\, p^{\nu}$, is still a good approximation for very low p ($\ll$ 100 Pa), such as on Mars. The value of A depends on the properties of the adsorber, e.g. on its specific surface area, and ν is an empirical constant related to the heterogeneity of the adsorbing material (Zent and Quinn, 1997). For varying temperatures basic thermodynamics can be applied leading to the Clausius-Clapeyron-like van't Hoff equation (1), which, for adsorption in equilibrium (as many molecules attaching as leaving the surface), links p and T:

(1) $$\frac{\partial \ln p}{\partial (1/T)} = -\frac{H}{R}$$

Here H is enthalpy of the reaction and R is the universal gas constant (8.314 J/mol/K). Hence standard-form $a(p,T)$-expressions and theories of adsorption (such as Langmuir and BET) use $p{\cdot}exp(\varepsilon/T)$ as the variable, $\varepsilon = H/R$ being a measure of the molar bonding energy of physisorption. Physisorption is generally favored by low p and is considered nonspecific with low enthalpies (5-40 kJ/mol), whereas chemical adsorption (chemisorption) is strongly material-dependent and is associated with high p and high enthalpies. In chemical engineering physisorption into e.g. the strongly adsorbing crystallized aluminosilicates (zeolites) is used for many applications.

3. Measurements for Mars

For Mars, adsorption of water vapor was suggested by e.g. Fanale and Cannon (1971). Their adsorption isotherm FC71 was based on basalt powder measurements in the high temperatures (for Mars) of 250-300 K. They defined $a(p,T) = \rho_r{\cdot}\beta\, p^{0.51} exp(\varepsilon/T)$, where ρ_r is density of the regolith (~1500 kg m^{-3}), $\beta = 2.043{\cdot}10^{-8}$ Pa^{-1} and $\varepsilon = 2679.8$ K. This adsorption isotherm has been widely used. Zent and Quinn (1995, 1997) made measurements of adsorption of H_2O onto palagonites in more Mars -like conditions and Jakosky et al. (1997) applied their best-fit result. For very low p, as on Mars, their expressions ZQ97 and J97 can be simplified to the standard Freundlich form $a(p,T) = \rho_r A_s M_w (K_o{\cdot}p{\cdot}exp(\varepsilon/T))^{\nu}$, where A_s is the specific surface area of the adsorber and M_w ($2.84{\cdot}10^{-7}$ kg m^{-2}) is the surface mass density for a monolayer of water molecules. In J97 (ZQ97) A_s is 100 (17) $m^2\, g^{-1}$, K_o is 15.7 (7.54) $\cdot 10^{-9}$ Pa^{-1}, ε is 2573.9 (2697.2) K, and ν is 0.48 (0.4734). These last two isotherms indicate weak enthalpies εR of 21.4 (22.4) kJ mol^{-1} for adsorption, whereas enthalpy for frost formation and sublimation is a lot larger, 51.1 kJ mol^{-1}.

In contrast, the FC71 isotherm is not of the standard Freundlich form. We hence suggest a new such form, by defining a modified FC71 via:

(2) F71m: $$a(p,T) = \rho_r{\cdot}\beta{\cdot}\gamma(p{\cdot}exp(\varepsilon/T))^{0.51}$$

where β and ε are the same as in the original FC71 and $\gamma = \exp(\varepsilon/270K)/(\exp(\varepsilon/270K))^{0.51} = 129.46$. At the high measurement temperatures of ~270 K the modified FC71m (2) therefore equals

FC71, but extrapolation to the low nocturnal Mars temperatures now obeys the van't Hoff equation (1), as it should. These four analytic isotherms FC71, J97, ZQ97 and FC71m will be tested against the PHX observations in section 4.

There are also measurements of adsorption in Mars-like conditions, which are not given in an analytic form. For instance Nikolakakos and Whiteway (2018) report strong adsorption of water vapor to zeolites but very little to quartz sand. Pommerol et al. (2009) made comprehensive measurements at 243 K on six Mars-analog soil samples, which resemble many types of orbit-recognized martian surface mineralogy. A wide range of adsorption for the same p was observed in these samples, with some hysteresis between adsorption and desorption. Beck et al. (2010) then considered the debated timescales of adsorption kinetics using these measurements. They estimate the kinetics to be relatively fast at 243 K (about 10-100 s) but perhaps slower (a few hours) at 200 K. Chevrier et al. (2007) and Bryson et al. (2008) measured adsorption and desorption through basaltic dust (JSC-1) at 270 K, finding it to be efficient and rapid at that high temperature.

The above and other measurements to various candidate martian adsorbers thus reveal quite diverse results. Yet the REMS observations along the Curiosity track (Fig. 1) suggest rather homogeneous daily minima of vmr. Furthermore, in all the adsorptive UH/FMI SCM simulations for Curiosity (Savijärvi et al.. 2016, 2019a,b, 2020a), the same palagonite-based isotherm (J97) has produced a decent fit to the observed minima of vmr, despite the fact that the rover had certainly traversed quite different soils. Steele et al. (2017) presented mesoscale model results for Curiosity. Their model-vmr also indicates an approximate match with the REMS vmr minima for two isotherms (ZQ97, J97) during three L_s periods in two years, i.e. at six different sites. Could the recalibrated Phoenix data and modeling perhaps help to explain the controversy?

4. Modeling experiments for Phoenix sols 48-60

We now return to the Phoenix midsummer sol 50-60 case of Savijärvi et al. (2020b), as frost was practically nonexistent during this period and the recalibrated Fischer et al. (2019) TECP data appear to give a good representation of the diurnal cycle in the water vapor pressure p. We add here data from sols 48-49 to get some more in-air TECP observations of p. The observed air pressure P varied only very slightly (788.9-799.3 Pa) during these PHX sols (48-60; L_s 97.5^o-103^o). Hence a constant value P_o = 794 Pa is adopted in the following for simplicity.

The atmosphere-subsurface SCM and its initialization is the same as in Savijärvi et al. (2020b). Since we concentrate here on the adsorption isotherms, only the model's soil moisture aspects are briefly described below. The model's moisture variable is the water vapor mass mixing ratio q ($q = 0.41 \cdot vmr = 0.41 \cdot p/P$). There are 30 grid points in the air column (0.3, 0.8, 2.0, 5.0 m, … to 30 km) and eight grid points in the soil at depths of 0, 0.25, 0.5, 2.0, 3.8, …, 35 cm. Vertical diffusions of soil temperature T_s and pore air mixing ratio q_s are solved at these depths in 10 s time steps, taking into account adsorption, ground frost and pore ice. Air density in the pores is $\rho_s(z) = P_o/(R_{CO2}T_s)$. Porosity (air fraction) f of the regolith is 16%, thermal inertia 150 SI units and surface albedo 0.18. Below 5 cm depth the soil pores are filled with ice, as observed by PHX (Smith et al., 2009). The initial air-q -profile is linear (as indicated by GCMs), integrating to the observed PWC ~30 μm of

192 the period. The model is run to sol 3, when it keeps repeating its diurnal cycles of winds,
193 temperatures and moistures. The results shown are from this last sol.

194 Soil moisture is assumed to exist in the regolith both as water vapor in the pores (with density fw =
195 $fq_s\rho_s$) and as adsorbed water $a(fw,T)$ on the grain surfaces. For a unit volume of regolith, then

196

197 (3) $\frac{\partial}{\partial t}\left(fw + a(fw,T)\right)$ = vertical diffusion of w through the porous regolith

198 Assuming that f is constant and air temperature in the pores adopts the predicted T_s but its density
199 changes are negligible, this leads to the model's prediction equation (4) for q_s:

200 (4) $$\frac{\partial q_s}{\partial t} = \frac{1}{fc}\frac{\partial}{\partial z}\left(D_e\frac{\partial q_s}{\partial z}\right) - \frac{1}{\rho_s fc}\frac{\partial a(fw,T_s)}{\partial T_s}\frac{\partial T_s}{\partial t}$$

201 where D_e is effective diffusivity of vapor in the porous soil and $c = 1 + (1/f)\,\partial a(fw,T_s)/\partial w$. At
202 each time step, after the update of $T_s(z)$ (and of ρ_s, c and D_e), $q_s(z)$ is first updated by the last
203 adsorption term of (4). Then q_s is updated at the surface by matching the current flux from the
204 ground with flux to the atmosphere, and this is used as the top boundary condition in solving the
205 vertical diffusion part of (4). Finally conditions for super- and subsaturation are checked in the soil
206 and amounts of surface frost and pore ice are updated accordingly. For D_e the Buckingham rule D_e
207 $= f^2D$ is adopted; the molecular diffusion coefficient $D(P,T)$ of H_2O in CO_2 (~ 10^{-4} m^2/s) is from
208 Wallace and Sagan (1979) (as in Hudson et al., 2007), and $\partial a(fw,T_s)/\partial w$, $\partial a(fw,T_s)/\partial T_s$ are
209 estimated by finite differencing. By ideal gas law, in-soil p for the $a(p,T)$-applications of section 3 is
210 $p = fwR_wT_s$, where R_w is the specific gas constant of water vapor, 461 J kg^{-1} K^1.

211 The model is applied here for Phoenix at L_s 101° (sol 55) with parameter values as listed in
212 Savijärvi et al. (2020b). The simulated 2 m day and night wind speeds are similar to the PHX
213 telltale readings as in Savijärvi and Määttänen (2010). The simulated air temperatures at 2 m height
214 produce a near-perfect match (bias 0.15 K, standard deviation (std) 3.6 K) with the observed MET-
215 mast temperatures during the period (Fig. 2) so the model's ground temperatures T_g and the other
216 $T_s(z)$ (T_s at 2 cm depth shown in Fig. 2 for later reference) presumably correctly represent the
217 apparent average soil temperatures around the lander. The temperatures are the same in simulations
218 with the various adsorption isotherms. The TECP-derived frost points T_f are well below *T2m* and
219 T_s(2cm) in Fig. 2, so neither fog nor pore ice is expected during the period while weak ground frost
220 ($T_g \leq T_f$) might occur only shortly during the coldest hour, if at all.

221 The hourly TECP vapor pressures p are shown in Fig. 3 in log scale, all near-surface observations at
222 ~ 3 cm height being filled squares, and all in-air values (at 0.48-1.11 m heights, when indicated in
223 Zent et al., 2010), open squares. A clear diurnal cycle 0.04 - 1 Pa can be seen, estimated errors
224 being ±0.005 Pa for the low nocturnal values and ±0.30 Pa for the high midday values (Fischer et
225 al., 2019). Five model simulations are also shown in Fig. 3. The model's surface-p curves using the
226 J97, ZQ97 and FC71m isotherms are so close to each other that they fall together in Fig. 3. They are
227 also close to the observations, an exception being the midday period, when the observed near-
228 surface-p -values are higher than in the model for an unknown reason. The 43 air-p observations
229 (open squares) are, however, quite close to these three model curves even during midday, model

bias being below 0.008 Pa and std 0.062, 0.060 and 0.068 Pa for J97, ZQ97 and FC71m respectively. Furthermore, in these three simulations PWC is conserved from sol to sol (as was observed) at around 30 μm, for *f* of 16%. The low value of porosity is consistent with the crusty nature of the top regolith reported for Phoenix (Smith et al., 2009). The model-indicated porosity is 35-40% at the Gale crater base (Savijärvi et al., 2016; Steele et al., 2017), whereas 45% was reported for the Negev desert site in Israel.

The FC71 PHX simulation (short dashes) displays instead excessive *p*-values in Fig. 3, and it does not conserve PWC for any realistic porosity. There is also a no-adsorption simulation (dash-dots), where *a(fw,T)* is set to 0 in (4). Here the remaining unscaled diffusion (c = 1) weakly depletes water vapor from the moist air to the soil during the day, until from about 2130 LMST (local mean solar time) frost point is reached and air moisture is strongly depleted to ground frost. Frost then sublimates in the morning sunshine and is gone by 0515 LMST, allowing for the weak diffusion to continue.

Figure 4 shows the surface fluxes in the integrations (except for FC71, where it is excessive). The fluxes are fairly similar for J97, ZQ97 and FC71m: upward during 0900-1700 LMST with maximum around 1300-1400 LMST, and downward outside these hours. In the no-adsorption experiment the flux is weakly downward, being upward only during the short sublimation period.

Figure 5 shows the adsorbed amounts of water in weight-% of soil for the three standard-form isotherms at the surface (thick lines), and at 2 cm depth (thin lines). The J97 and FC71m simulations produce strikingly similar diurnal cycles. Their patterns are quite similar to the Negev desert measurements of gravimetric soil water content in the 0-1 and 2-3 cm depth layers (Agam and Berliner, 2004) but values are, of course, much smaller in Mars. The ZQ97 simulation produces small values of adsorbed water (as in Steele et al., 2017) because its specific surface area A_s (17 m^2g^{-1}) is much smaller than in J97 (100 m^2g^{-1}). Nevertheless, the ZQ97 surface vapor pressures and fluxes to the atmosphere are nearly the same as in J97, by Figs. 3-4. All the 2 cm depth curves are rather flat in Fig. 5, so the diurnal adsorptions and desorptions are strongly concentrated to the top 1 cm of regolith, as shown in Steele et al. (2017) and Savijärvi et al. (2020b).

Figure 6 displays the pore water vapor concentrations *fw* at the surface and at 2 cm depth. The three thick surface lines are nearly identical with a midday maximum but low *fw* at night, when a lot of the vapor has been depleted to the adsorbed mode. At 2 cm depth the J97 and FC71m curves are close to each other with a damped and delayed maximum, similarly to the 2 cm T_s curve in Fig. 2. In contrast the ZQ97 afternoon maximum of *fw* is higher at 2 cm than at the surface. The reason is that, adsorbed amount being so small in ZQ97 (Fig. 5) due to the small A_s, more of the moisture can now stay in the vapor mode at the 2 cm depth. At the surface the diurnal adsorption cycle was instead independent of A_s. This will be explained in the next section.

In summary, the results with the suggested FC71m (Eq. 2) appear to be quite close to the PHX observations and also to those obtained with J97 and ZQ97. This presumably means that the FC71 measurements of H_2O adsorption to basalt were quite good at the high ~270 K temperature of those measurements, but extrapolation to lower temperatures is improper in the original FC71. Eq. (2) appears to fix that and therefore FC71m is recommended instead of FC71.

For J97 and ZQ97 the model actually applies the original, more complex Langmuir-type isotherms. The results remain, however, exactly the same when using the simplified Freundlich forms of section 3, because of the very low values (< 1 Pa) of vapor pressure.

The opposite and reversible diurnal variations in the soil water column and PWC are about 1% of PWC in the simulations with the three Freundlich isotherms J97, ZQ97 and FC71m. Interestingly, the same ~1% of PWC was found in the Negev desert. Adsorbed amounts of water in the topsoil are, however, much smaller at PHX than at Negev, related to the much smaller values of available moisture and smaller porosity. The adsorbed amounts depend strongly on the adsorption isotherm chosen (Fig. 5), yet the associated surface fluxes and the resulting values for surface-*p* are very nearly the same (Figs. 3-4). This means that observations of air moisture alone are not enough to reveal the water amounts in the soil. Proper soil moisture measurements or sample returns are needed instead. The reason for this is discussed next.

5. Discussion

In the porous soil $p = fw\mathrm{R_w}T_s \sim fw\mathrm{R_w}\mathrm{T_o}$, where $\mathrm{T_o}$ is a constant temperature ~220K. All the four analytic isotherms *a(p,T)* considered in section 3 can hence be presented in an approximate generic form for *a(fw,T)*, by substituting $p = fw\mathrm{R_w}\mathrm{T_o}$ to them:

(5) $$a(fw, T) = Aw^{\alpha v}\exp(\varepsilon v/T)$$

Here A combines all the *w*- and *T*-independent constants, e.g. *f*, $\mathrm{R_w}$, $\mathrm{T_o}$ and the assumed specific surface areas $\mathrm{A_s}$ and densities of regolith. For FC71m, J97 and ZQ97 $\alpha = 1$ and ε and v are as given in section 3, whereas in FC71, $\alpha = 0.51$, $\varepsilon = 2679.8$ K and $\nu = 1$. Since $\partial a/\partial w$ is of the order of 10^6 (>> 1) by all four isotherms and hence $c \cong (1/f)\partial a/\partial w$ when adsorption is active, the last term in the model's prediction equation (4) is, after substituting *c* and (5), and then differentiating analytically:

(6) $$\frac{\partial q_s}{\partial t} = \cdots \quad -\frac{1}{\rho_s f c}\frac{\partial a}{\partial T_s}\frac{\partial T_s}{\partial t} \cong -\frac{1}{\rho_s}\frac{\partial a/\partial T_s}{\partial a/\partial w}\frac{\partial T_s}{\partial t} \approx -\frac{1}{\rho_s}\left(-\frac{\varepsilon}{\alpha}\frac{w}{T_s^2}\right)\frac{\partial T_s}{\partial t}$$

Thus A and ν cancel out completely! Hence the adsorption term is effectively independent of the specific surface area, heterogeneity and density of regolith. The only remaining parameter is ε/α. This now explains why the three standard-form isotherms with quite different $\mathrm{A_s}$ but fairly similar ε produce nearly identical *p*-curves for PHX in Fig. 3, and why the observed daily MSL minima of *vmr* (due to the daily adsorption) of Fig. 1 are independent of ground mineralogy along the Curiosity track, depending only on the current PWC, ground temperature and porosity. In other words, equilibrium-based adsorption to regolith appears nonspecific on Mars.

Another explanation would be, of course, that winds blow similar dust all over Mars into a globally uniform regolith. It is, however, hard to believe that the regolith would be exactly the same in such distant spots as PHX (68°N), the Gale crater (5°S) and the two Viking sites (24°N, 48°N; Savijärvi et al., 2018), in all of which the UH/FMI SCM with the same adsorption isotherm has provided moisture simulations, which agree with the available direct and indirect observations.

We note in passing that Eq, (6) also helps to understand the failure of FC71. In FC71 the effective enthalpy is $(\varepsilon/\alpha)R$ = 43.7 kJ/mol; i.e. twice that in the other three isotherms and closer to the strong enthalpy of sublimation (51 kJ/mol). As a result, the FC71 simulation rapidly removes moisture from soil to the atmosphere by strong desorption (Fig. 3), daytime convection then mixing it higher up every sol. PWC therefore grows rapidly and unrealistically from sol to sol in this simulation; from the initial 30 μm to about 50 μm by sol 5.

The diffusion term of (4) is somewhat sensitive to A through the scaler 1/c. But as c is quite large, ~10^6, diffusion is strongly damped when adsorption is active (Zent et al., 1993; $D_e/c \sim 10^{-10}$ m^2/s). Hence the nocturnal adsorption slows down diffusion of water vapor in the topsoil, by temporarily removing pore moisture to the grain surfaces. This also means that the exchange with the ice table at 5 cm is practically nonexistent in the diurnal time scale. Even when unscaled, the daily diffusion remains relatively weak, as seen in the no-adsorption case curves of Figs. 3-4.

Since the model's surface water vapor pressure with the three standard Freundlich form isotherms is so close to the observed (Fig. 3), its prediction equation for q_s (4) appears realistic. On the other hand, the surface air pressure was nearly constant during PHX sols 48-60, so that $q_s \sim b \cdot p$ and $w \sim b \cdot p \cdot \rho_s$, where $b = 0.41/P_o$ is a constant. Substituting these to (4), dropping the tiny diffusion term and making use of (6) for the standard-form isotherms (α=1) leads to

$$\frac{\partial p}{\partial t} \cong \frac{\varepsilon p}{T_s^2}\frac{\partial T_s}{\partial t} \qquad (7)$$

at each depth. Rearranging, this gives for p at the surface

$$\partial(\ln p_g) \cong -\varepsilon\, \partial(1/T_g), \qquad (8)$$

which can also be obtained directly and accurately from the van't Hoff equation (1) for adsorption in equilibrium. Thus, if the observed values of surface-*ln(p)* of Fig. 3 are plotted against simultaneous $1/T_g$ from the model (Fig. 2) during strong adsorption and desorption, these pairs should fall onto a straight line of slope -ε. Indeed they do, and a least square fit produces during 1800-2100 LMST, ε of 2686 ± 20 K for adsorption, and during 0600-0900 LMST, ε of 2700 ± 20 K for desorption (displaying almost no hysteresis in the PHX sol 48-60 data). Lab-based ε in the four analytic adsorption isotherms of section 3 are close to these values. Enthalpies H = εR become, respectively, 22.3 and 22.4 kJ/mol. Initial MSL REMS observations were similarly used in Savijärvi et al. (2015), producing at Gale a tentative first-guess enthalpy in the range of 20-22 kJ/mol. Independently assessed enthalpies from the MSL REMS p,T_g -measurements by Rivera-Valentin et al. (2018) are close to these values.

In the model we have assumed that adsorption and desorption are fast processes, being instantaneously in equilibrium and hence obtainable at any time step from the current fw_s and T_s. The results appear to be consistent with this approximation, as the model's p-curve fits quite well to the observations, even during the cold night (T_g ~ 191 K), when adsorption kinetics might be thought to slow down. Beck et al. (2010) have estimated the timescales of adsorption kinetics to be about 50 s in a ferrihydrate sample at 243 K, but about 10000 s (2.7 martian hours) at 200 K, for

346 enthalpy of 50 kJ/mol. However, if enthalpy is instead ~ 22 kJ/mol, as suggested above, their fig. 8
347 indicates that the time scale at 200 K then is much faster; about 500 s or only about 8 martian
348 minutes. Thus adsorption/desorption would be close to equilibrium in the time scale of less than an
349 hour all the time.

350

351 **6. Concluding remarks**

352 The *in-situ* near-surface moisture observations of MSL and PHX indicate strong diurnal adsorption
353 and desorption, which appears insensitive to adsorption isotherms used in modeling, and also
354 insensitive to the varying mineralogy of regolith along the long Curiosity track. To explain this, a
355 series of model simulations was performed using for validation the recalibrated PHX/TECP data of
356 Fischer et al. (2019). The warm midsummer PHX sol 48-60 period was selected, when observations
357 reveal a strong diurnal cycle in the near-surface water vapor partial pressure *p* without fog or
358 significant frost. The column model assumes instantaneous adsorption in equilibrium. It is the same
359 as described and used in Savijärvi et al. (2020b) for PHX, but here four different adsorption
360 isotherms are tested and the soil moisture aspects are considered in detail. Comparison is also made
361 to theory and to Earth observations of daily water vapor adsorption in the Negev desert of Israel.

362 The model produces an excellent simulation of the observed diurnal 2 m PHX temperatures, so that
363 its ground surface and in-soil temperatures are presumably also accurate. When applying the
364 adsorption isotherms of Zent and Quinn (1997) and Jakosky et al. (1997) for palagonites, the
365 resulting diurnal surface water vapor pressure curves are nearly identical to each other and quite
366 close to the recalibrated values, despite the fact that the assumed specific surface areas for regolith
367 differ by a factor of 6 in these two isotherms.

368 In contrast, adopting the widely used Fanale and Cannon (1971) isotherm for basalt results in
369 excessive values for *p*. However, when FC71 is modified to a standard Freundlich form (so that it,
370 like J97 and ZQ97, obeys the van't Hoff law (Eq. 1) for adsorption in equilibrium), the results are
371 excellent and nearly identical to those from J97. We hence recommend the use of the modified form
372 (FC71m, Eq. 2) for all applications, instead of the original. The problem in the original FC71 is in
373 an inappropriate extrapolation to the low nighttime temperatures of Mars.

374 When analyzing the model's prediction equation it turned out that with all three standard-form
375 isotherms its adsorption term closely follows the van't Hoff equilibrium law and the only important
376 parameter is the enthalpy H of adsorption, which is quite similar (~22 kJ/mol) in the three excellent-
377 match schemes. In contrast, the effective enthalpy is nearly double in the original FC71, which
378 explains its excessive behavior.

379 Even more importantly, all the other properties of regolith except enthalpy, such as density,
380 heterogeneity and specific surface area, are reduced away from the model's adsorption term. Thus,
381 under the assumption of equilibrium- and non-kinetic -based physisorption, the result is that
382 material dependencies weaken. Hence adsorption appears largely nonspecific in the diurnal time
383 scale, being independent of the properties of the regolith, except enthalpy (and porosity, which
384 governs the surface exchange). The good equilibrium-model match with the observed diurnal water

vapor pressure cycle suggests that adsorption and especially desorption are relatively fast processes. Therefore instantaneous equilibrium appears to be a useful approximation for atmospheric models, if detailed information of adsorption kinetics is not specifically needed.

As a result, the diurnal surface fluxes are nearly equal for the three standard Freundlich form isotherms J97, ZQ71, F71m. The resulting diurnal and opposite variation in the column soil water and PWC due to the adsorption cycle is only about 1% of PWC in all these three simulations, because air moisture is depleted in a quite shallow ~200 m deep nocturnal air layer (Savijärvi et al., 2016; 2020b). Interestingly, the diurnal variation in the column soil water was also about 1% of PWC in the Negev desert observations of Agam and Berliner (2004). The adsorbed water amounts are of course very much smaller on Mars, particularly so for ZQ71, due to the small specific surface area assumed in it.

Finally, the van't Hoff plot of the observed $ln\ p$ vs. model's $1/T_g$ during periods of strong adsorption and desorption suggests H of about 22.3 and 22.4 kJ/mol, respectively. Thus the TECP observations indicate low enthalpy and no significant hysteresis. In conclusion the water vapor adsorption on present-day Mars is associated with very low partial pressures and low enthalpies, and appears essentially nonspecific to the adsorber (e.g., mineralogy of regolith). All these are typical features of physisorption in general.

Acknowledgements:

The work is supported by the Academy of Finland grants 131723, 132825 and 310509.We are grateful to Erik Fischer, German Martinez and the University of Michigan team for lending their new PHX/TECP data. Thoughtful comments and suggestions from the reviewers helped to improve the article.

References:

Agam N, Berliner PR, 2004. Diurnal water content changes in the bare soil of a coastal desert. J Hydrometeorology 5, 922-933.

Beck P, Pommerol A, Schmitt B, Brissaud O, 2010. Kinetics of water adsorption on minerals and the breathing of the Martian regolith. J. Geophys. Res. 115, E10011.

Bryson KL, Chevrier V, Sears DWG, Ulrich R, 2008. Stability of ice on Mars and the water vapor diurnal cycle: Experimental study of the sublimation of ice through a fine-grained basaltic regolith. Icarus 196, 446-458.

Böttger HM, Lewis SR, Read PL, Forget F, 2005. The effects of the martian regolith on GCM water cycle simulations. Icarus 177, 174-189.

Chevrier V, Sears DWG, Chittenden JD, Roe LA, Ulrich R, Bryson K, Billingsley L, Hanley J, 2007. Sublimation rate of ice under simulated Mars conditions and the effect of layers of mock regolith JSC Mars-1. Geophys. Res. Letters 34, L02203.

Fanale FP, Cannon WA, 1971. Adsorption on the Martian regolith. Nature 230, 502-504.

Fischer E, Martínez GM, Rennó NO, Tamppari LK, Zent AP, 2019. Relative humidity on Mars: new results from the Phoenix TECP sensor. J. Geophys. Res. 124, 2780-2792.

Gomez-Elvira J et al., 2012. REMS: the environmental sensor suite for the Mars Science Laboratory rover. Space Sci. Rev. 170, 583-640.

Harri A-M et al., 2014. Mars Science Laboratory relative humidity observations: initial results. J. Geophys. Res. Planets 119, 2132-2147, doi: 10.1002/2013JE004514

Hudson TL, Aharonson O, Schorghofer N, Farmer CB, Hecht MH, Bridges NT, 2007. Water vapor diffusion in Mars subsurface environments. J.Geophys.Res. 112, E05016.

Jakosky BM, Zent AP, Zurek RW, 1997. The Mars water cycle: Determining the role of exchange with the regolith. Icarus 130, 87-95.

Martínez GM, et al., 2017. The Modern Near-Surface Martian Climate: A Review of In-situ Meteorological Data from Viking to Curiosity. Space Sci. Rev., pp. 1-44.

Masiello C, Serio C, Venafra S, De Feis I, Borbas EE, 2014. Day-night variation of Sahara desert sand emissivity during the dry season from IASI observations. J. Geophys. Res. 119, 1626–1638, doi:10.1002/jgrd.50863.

Nikolakakos G, Whiteway JA, 2018. Laboratory study of adsorption and deliquescence on the surface of Mars. Icarus 308, 221-229.

Paton M, Harri A-M, Mäkinen T, Savijärvi H, Hagermann A, Kemppinen O, 2016: Thermal and microstructural properties of fine-grained material at the Viking Lander 1 site. Icarus 271, 360-374, doi:10.1016/j.icarus.2016.02.012

Pommerol A, Schmitt B, Beck P, Brissaud O, 2009. Water sorption on martian regolith analogs: Thermodynamics and near-infrared spectroscopy. Icarus 204, 114-136.

Rivera-Valentin EG, Gough RV, Chevrier VF, Primm KM, Martinez GM, Tolbert M, 2018. Constraining the potential liquid water environment at Gale crater, Mars. JGR Planets 123,1156-1167.

Savijärvi H, Määttänen A, 2010. Boundary-layer simulations for the Mars Phoenix lander site. Quart. J. Roy. Met. Soc. 136, 1497-1505.

Savijärvi H, Harri A-M, Kemppinen O, 2016. The diurnal water cycle at Curiosity: role of exchange with the regolith**.** Icarus 265, 63-69, doi:10.1016/j.icarus.2015.10.008.

Savijärvi H, Paton M, Harri A-M, 2018. New column simulations for the Viking landers: winds, fog, frost, adsorption? Icarus 310, 48-53, doi: 10.1016/j.icarus.2017.11.007.

Savijärvi H, McConnochie T, Harri A-M, Paton M, 2019a. Annual and diurnal water vapor cycles at Curiosity from observations and column modeling. Icarus 319, 485-490. doi:10.1016/j.icarus.2018.10.008.

Savijärvi H, McConnochie T, Harri A-M, Paton M, 2019b. Water vapor mixing ratios and air temperatures for three martian years from Curiosity. Icarus 326**,** 170-175, doi:10.1016/j.icarus.2019.03.020.

Savijärvi H, Martinez G, Harri A-M, Paton M, 2020a: Curiosity observations and column model integrations for a martian global dust event. Icarus 337, 113515, doi:10.1016/j.icarus.2019.113515.

Savijärvi H, Martinez G, Fischer E, Renno N, Tamppari L, Zent A, Harri A-M, 2020b: Humidity observations and column simulations for a warm period at the Mars Phoenix lander site: constraining the adsorptive properties of regolith. Icarus 343, 113688.

Steele LJ, Balme MR, Lewis SR, Spiga A, 2017. The water cycle and regolith-atmosphere interaction at Gale crater, Mars. Icarus 280, 56-79.

Smith PH et al., 2009. H_2O at the Phoenix landing site. Science 325 (5936), 58-61. doi:10.1126/science.1172339.

Vasavada AR et al., 2017. Thermophysical properties along Curiosity's traverse in Gale crater, Mars, derived from the REMS ground temperature sensor. Icarus 284, 372-386.

Wallace D, Sagan C, 1979. Evaporation of ice in planetary atmospheres: Ice-covered rivers on Mars. Icarus 39, 385-400.

Zent AP, Haberle RM, Houben HC, Jakosky BM, 1993: A coupled subsurface-boundary layer model of water on Mars. J. Geophys. Res. 98, E2, 3319-3337. of water on Mars. J. Geophys. Res. 98, E2, 3319-3337

Zent AP, Quinn RC, 1995. Simultaneous adsorption of CO_2 and H_2O under Mars-like conditions and application to the evolution of the martian climate. J. Geophys. Res. 100, 5341-5349.

Zent AP, Quinn RC, 1997: Measurement of H_2O adsorption under Mars-like conditions: Effects of adsorbent heterogeneity. J. Geophys. Res. 102, E4, 9085-9095.

Zent AP et al., 2010. Initial results from the thermal and electrical conductivity probe (TECP) on Phoenix. J. Geophys. Res. 115, E00E14, doi:10.1029/2009JE003420Zent AP, Hecht MH, Hudson TL, Wood SE, Chevrier VF, 2016. A revised calibration function and results for the Phoenix mission TECP relative humidity sensor. J. Geophys. Res. Planets 121, 626-651.

Zent AP, Hecht MH, Hudson TL, Wood SE, Chevrier VF, 2016. A revised calibration function and results for the Phoenix mission TECP relative humidity sensor. J. Geophys. Res. Planets 121, 626-651

Figures:

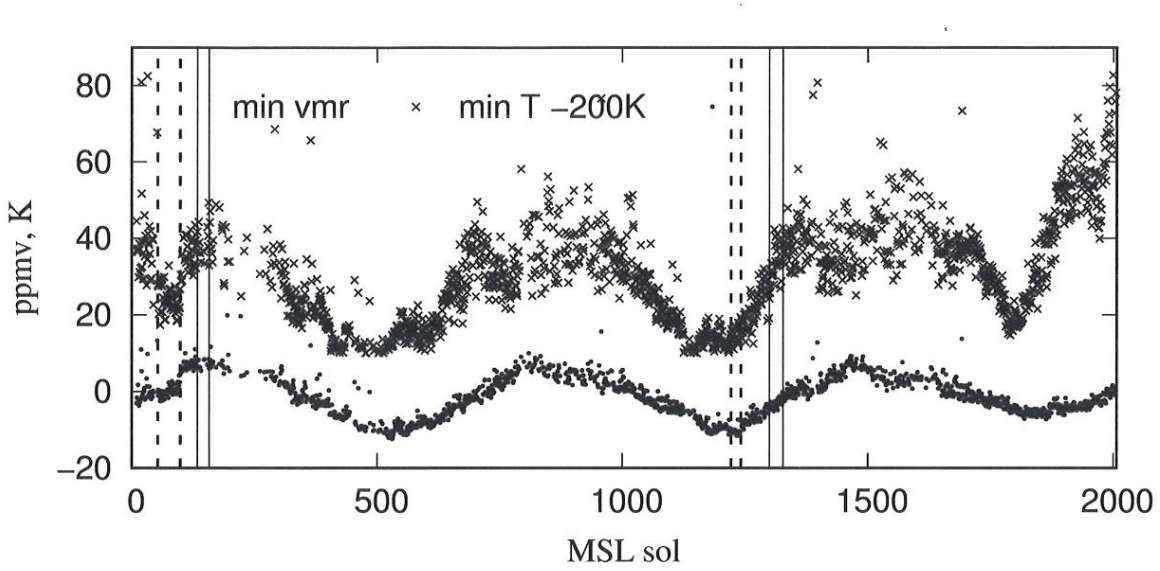

Figure 1. Crosses: The REMS-H daily minimum water vapor volume mixing ratios during three Mars years (min vmr, in ppmv). Dots: The REMS-H daily temperatures at the times of min vmr (min T minus 200 K, in K). Solid lines indicate two short rock-dominated periods and dashed lines two dune-dominated periods during the travel of Curiosity.

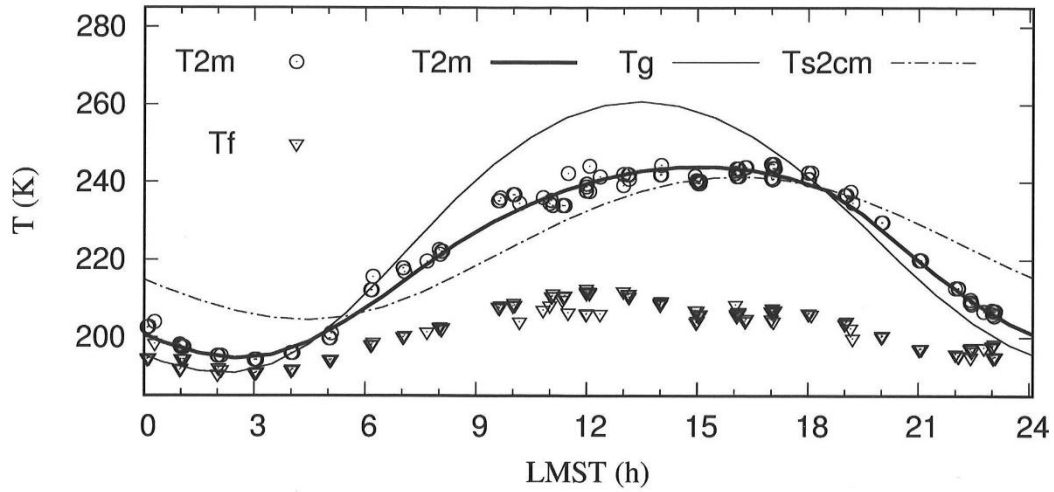

Figure 2. Observed diurnal Phoenix 2 m air temperatures (*T2m*, from MET-mast) and frost points (T_f, from TECP, Fischer et al., 2019) during PHX sols 48-60. Lines are sol 55 model values for *T2m*, ground temperature T_g, and T_{soil} at 2 cm depth. LMST = local mean solar time in Mars hours.

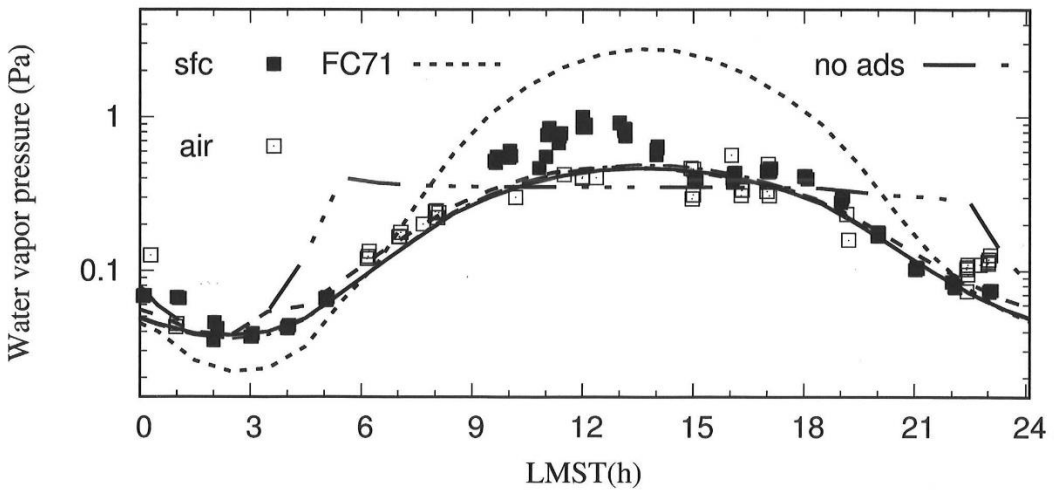

Figure 3. PHX/TECP water vapor pressures *p* (near-surface: filled squares, in-air: open squares) during PHX sols 48-60 (Fischer et al., 2019), and model-*p* at the surface (lines): no adsorption (dash - 3 dots); with FC71 isotherm (short dashes); with ZQ97 (long dashes); with J97 (solid). FC71m (dash-dots) is identical to J97 within the thickness of the solid line. PWC is about 30 μm.

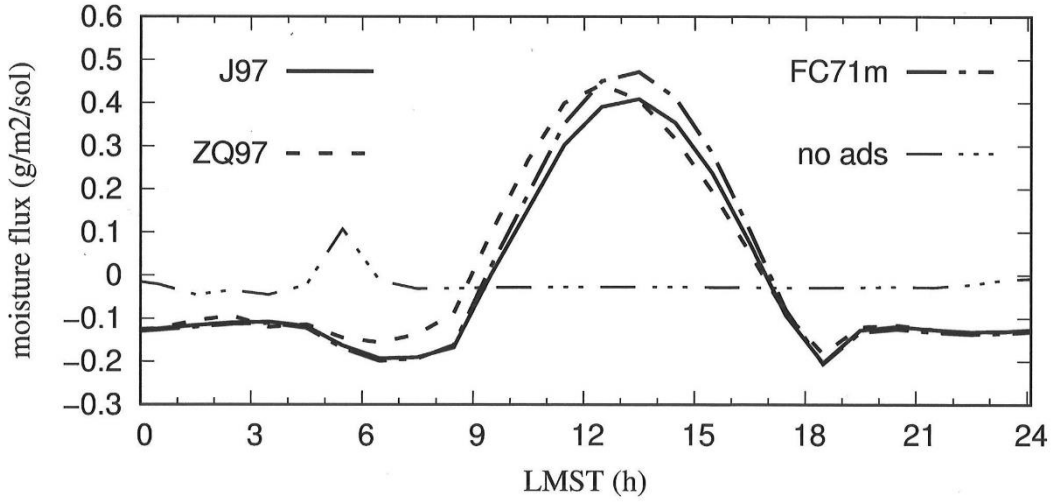

Figure 4. Surface fluxes of moisture (in g m^{-2} sol^{-1}, positive upward) in the four indicated PHX sol 55 simulations.

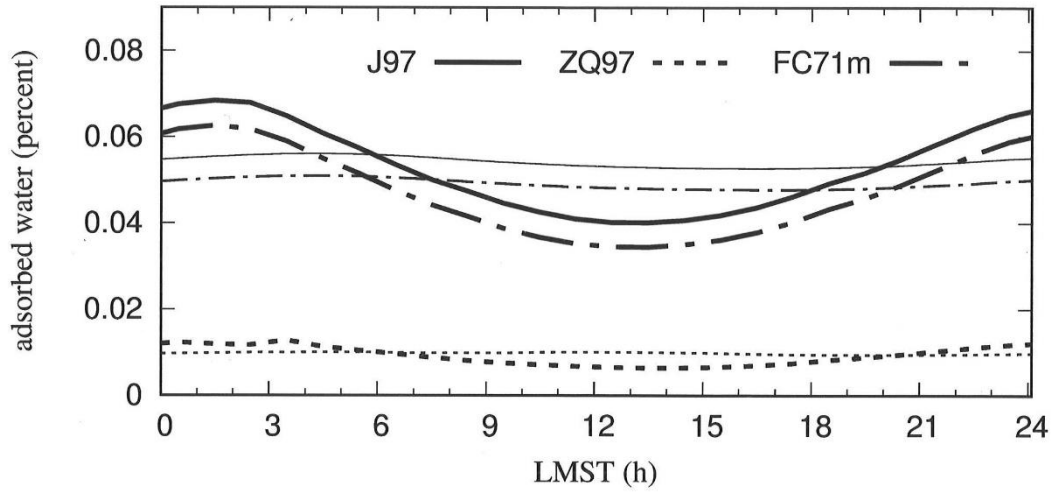

Figure 5. Adsorbed water amounts (in weight-% of regolith) at the surface (thick lines) and at 2 cm depth (thin lines) in the three indicated simulations.

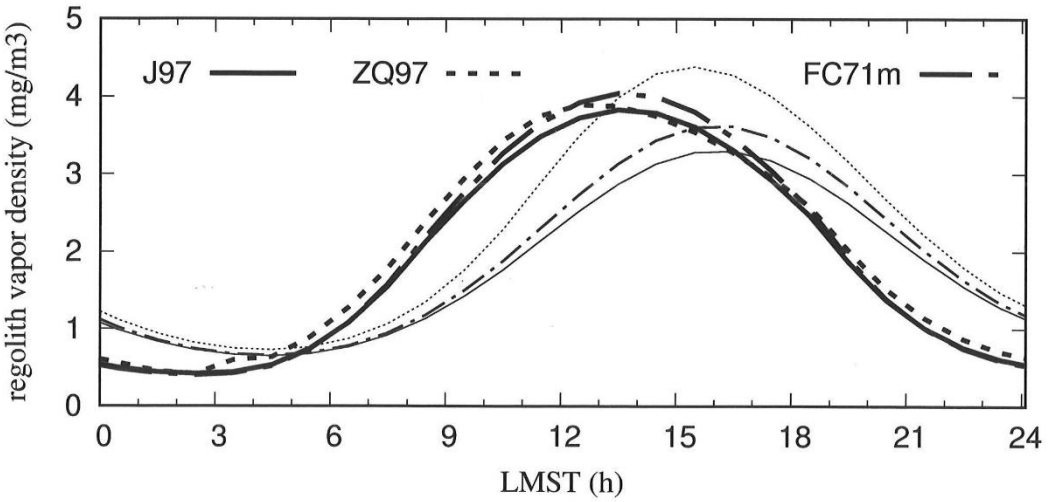

Figure 6. Water vapor densities *fw* (in mg per m^3 of regolith) at the surface (thick lines) and at 2 cm depth (thin lines) in the three indicated simulations.